

Dynamic Magnetic-Transformation-Induced Exchange Bias in [α -Fe₂O₃]_{0.1}[FeTiO₃]_{0.9}

P. Song,^{1,2} L. Ma,^{1,*} G.K. Li,¹ C.M. Zhen,¹ C. Wang,² E.K. Liu,³ W.H. Wang,³ J.L. Chen,³ G.H. Wu,³ Y.H. Xia,⁴ J. Zhang,⁴ C.M. Xie,⁴ H. Li,⁴ and D.L. Hou^{1,†}

¹Department of Physics, Hebei Advanced Thin Films Laboratory, Hebei Normal University, Shijiazhuang 050024, China

²Center for Condensed Matter and Material Physics, Department of Physics, Beihang University, Beijing 100191, China

³Beijing National Laboratory for Condensed Matter Physics, Institute of Physics, Chinese Academy of Sciences, Beijing 100190, China

⁴Key Laboratory of Neutron Physics, Institute of Nuclear Physics and Chemistry, China Academy of Engineering Physics, Mianyang 621999, China



(Received 2 April 2019; published 7 May 2019)

To date, for the known exchange-bias (EB) systems there has been one pinning phase and one pinned phase, and the pinning and pinned phases are inherent to the material and do not mutually transform into each other. Interestingly, we show here that EB is observed in a special system [α -Fe₂O₃]_{0.1}[FeTiO₃]_{0.9} (HI-9). Neutron powder diffraction and magnetic measurement confirm the following for HI-9: (i) two types of short-range antiferromagnetic (AFM) orderings coexist and serve as two pinning phases; (ii) the pinned phase is not intrinsic to the structure but can be dynamically produced from the pinning phase with the help of an external magnetic field. Consequently, two anomalous EB behaviors are observed: (i) both the coercivity (H_C) and the exchange-bias field (H_E) simultaneously decrease to zero at 30 K; (ii) for a high cooling field (H_{cool}), H_E decreases logarithmically with increasing H_{cool} . Using Arrott plots it is confirmed that the first-order magnetic phase transformation (FOMPT) from the AFM Fe²⁺ to ferromagnetic (FM) Fe²⁺ and the second-order magnetic phase transformation for the process whereby the FM Fe²⁺ align with the external-field direction coexist in HI-9. The Morin transition and FOMPT cause anomalous EB behaviors. This work may provide fresh ideas in the application of the EB effect.

DOI: 10.1103/PhysRevApplied.11.054018

I. INTRODUCTION

Exchange-bias (EB) effect is an “interface” effect, making systems show unidirectional anisotropy, which has many applications in present technologies, including spin valve [1], magnetoelectric switching [2,3], magnetic tunnel junctions [4], and magnetic recording [5]. To date, EB has been observed in many materials with different microstructures, including core-shell nanoparticles [6–8], inhomogeneous materials [9], coated antiferromagnetic single crystals [10,11], and thin films [12–14]. Besides, it has been clarified that the interface is constructed by two magnetic phases. One phase should have a stronger magnetic anisotropy serving as the pinning phase, the other phase would have a weaker magnetic anisotropy serving as the pinned phase. This is the case for EB in antiferromagnetic- (AFM-)ferromagnetic (FM) systems [15–19], ferrimagnetic- (FIM-)FM systems [20–22],

AFM-FIM systems [23], AFM-superferromagnetic (SFM) systems [24], spin-glass- (SG-)FM systems [25,26]. Recently, the exchange-bias systems involving two pinning phases have emerged, including the AFM-FM-AFM system [27] and the FM-AFM-AFM system [28–30], which enhances the tunability and application potential of the EB effect. The common feature of these EB systems is that the pinning and pinned phases are inherent to the material, and do not mutually transform into each other. Would the systems with more than one AFM and without FM show EB? Interestingly, our group has observed EB in the single-phase hematite-ilmenite solid solution [α -Fe₂O₃]_{0.1}[FeTiO₃]_{0.9} (referred to below as HI-9) [31]. Although EB has been studied in the Fe₂O₃-FeTiO₃ system [32], however, in the case of Ref. [32] the system is a natural mineral, which is composed of two independent phases rather than a single phase as in our case. The illustration in Fig. 1(a) shows the crystal structure and magnetic configuration relationship of α -Fe₂O₃, HI-9, and FeTiO₃. It is known that both α -Fe₂O₃ and FeTiO₃ have a long-range AFM ordering and their Néel temperatures

*majimei@126.com

†houdenglu@mail.hebtu.edu.cn

(T_N) are approximately 950 and 58 K, respectively [33,34]. Therefore, in HI-9, Fe^{3+} (red) between the neighboring layers, and Fe^{2+} (orange) separated by the nonmagnetic Ti^{4+} layers (gray) are AFM-coupled, and their spins are parallel to the c axis. Hereby, HI-9 has two types of AFM ordering and does not have FM ordering [31,35]. Therefore, the magnetic configuration of HI-9 is different from that of the previous EB systems [15–30]. Based on our previous work [31], Figs. 1(b)–1(d) show the schematic diagram of the magnetic structure in HI-9 under different external fields. Figure 1(b) shows that two types of short-range AFM orderings coexist when the external field is zero, and they together serve as the pinning phase. When the external field increases to the critical field, part of the AFM Fe^{2+} transforms into FM state, as a result, magnetization jumps [31] are observed, and the formed FM Fe^{2+} serves as the pinned phase as shown in Fig. 1(c). Finally, as seen in Fig. 1(d), all of AFM Fe^{2+} transform into FM state when the external field is large enough, the pinning phase of AFM Fe^{2+} totally vanishes and the pinned phase of FM Fe^{2+} reaches the maximum. Recently Fita *et al.* [36,37] also demonstrated that exchange bias can be observed in RFeO_3 ($\text{R}=\text{Nd}, \text{Er}, \text{Sm}$) single phase. However, the AFM ordering and the FM ordering are inherent, and they do not mutually transform from each other although there exists a spin reorientation of the FM ordering. Considering that HI-9 has two AFM ordering and the FM ordering could be obtained by the external field, it will be a good platform to study EB.

In this paper, two types of short-range AFM ordering, a “two pinning phases and one pinned phase” (TPPOPP) structure, and the field-induced dynamic magnetic transformation between the pinning and pinned phases are evidenced by the neutron powder diffraction (NPD) and magnetic measurement. Two anomalous EB behaviors are observed: (i) both the coercivity (H_C) and the exchange-bias field (H_E) simultaneously decrease to zero at 30 K; (ii) for a high cooling field (H_{cool}), H_E decreases logarithmically with increasing H_{cool} . By application of Arrott plots, it has been confirmed that the above phenomena are related to the spin reorientation of Fe^{3+} (Morin transition) and the first-order magnetic phase transformation (FOMPT).

II. EXPERIMENTAL DETAILS

The HI-9 sample is prepared using a solid-state reaction method. Ground powders of FeTiO_3 (99.98%, Alfa Aesar Corporation) and $\alpha\text{-Fe}_2\text{O}_3$ (99.99%, Alfa Aesar Corporation) are fully mixed and sintered at 1473 K for 12 h and cooled slowly to room temperature. The NPD experiments are carried out at various temperatures using a high-resolution neutron powder diffractometer (HRND) ($\lambda = 1.884 \text{ \AA}$) at China Mianyang Research Reactor. Powder XRD patterns with Cu-K α radiation are obtained ranging from 20 to 300 K. Crystal structures are determined by

the Rietveld refinement method with the General Structure Analysis System [38]. To measure the magnetic properties of the powders, the sample is compressed into a nonmagnetic capsule. The magnetic measurements are performed in the temperature range from 2 to 300 K using a Physical Property Measurement System (PPMS-9, Quantum Design).

III. RESULTS AND DISCUSSION

A. Field-induced dynamic magnetic transformation of the TPPOPP structure in the AFM-AFM coupled system of HI-9

Figures 2(a) and 2(b) show the NPD patterns and magnetic hysteresis loop of HI-9 at room temperature (300 K) and low temperature (5 K), respectively. Rietveld analysis including occupancy refinement is performed to fit the NPD data. The fitted results confirm that HI-9 does have the crystal structure as shown in Fig. 1(a), and the occupancy of the Fe^{3+} cations in the Fe^{2+} and Ti^{4+} layers is 0.091 and 0.109, respectively. Most importantly, it is found that there is no contribution from magnetic scattering to the Bragg peaks at either room temperature or low temperature, suggesting that there is no long-range magnetic ordering throughout the entire temperature range, which is consistent with the short-range AFM ordering of the system [39–41]. However, the magnetic hysteresis loops of HI-9 at room temperature and low temperature are very different, unlike the case of NPD. There is no magnetic hysteresis at 300 K, but the obvious hysteresis is observed at 5 K and the saturation magnetization is as high as $2.22 \mu_B/\text{Fe}$, suggesting the existence of the long-range FM ordering.

Figure 2(c) shows the temperature dependence of the normalized relative lattice constants $(c - c_{300\text{K}})/c_{300\text{K}} = \Delta c/c_{300\text{K}}$ and $(a - a_{300\text{K}})/a_{300\text{K}} = \Delta a/a_{300\text{K}}$ based on the refinements of the variable-temperature NPD and XRD data. It can be seen that $\Delta a/a_{300\text{K}}$ almost linearly decreases with decreasing temperature, thus exhibiting a normal positive thermal expansion behavior, while $\Delta c/c_{300\text{K}}$ also decreases linearly initially, but an abnormal negative expansion occurs for temperatures lower than approximately 100 K, and this behavior becomes more pronounced for temperatures lower than approximately 30 K. According to our previous work [31] and Burton *et al.*’s work [42], approximately 100 K corresponds to the magnetic transformation temperature of the Fe^{2+} sublattice from the paramagnetic (PM) phase to the PM’ state, which is a subfield of the PM phase. On the other hand, approximately 30 K corresponds to the Morin transition temperature (T_M) (see parts 1 and 2 of the Supplemental Material for the verification of T_M [43]) of the Fe^{3+} sublattice, i.e., the Fe^{3+} cations will transform from the canted AFM [see illustration in Fig. 2(a)] perpendicular to the c axis to the collinear AFM [see illustration in Fig. 2(b)] parallel to the c axis

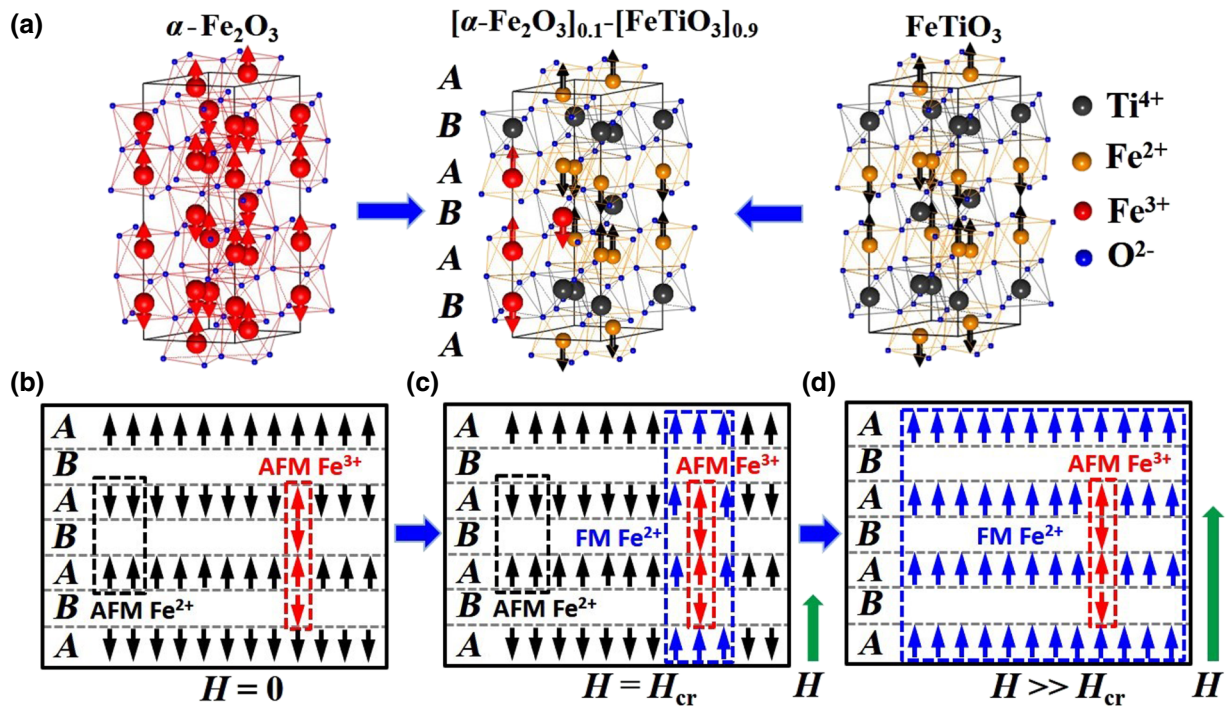


FIG. 1. (a) Illustration of the crystal structure and magnetic configuration of the hematite ($\alpha\text{-Fe}_2\text{O}_3$), ilmenite (FeTiO_3), and their solid solution ($[\alpha\text{-Fe}_2\text{O}_3]_{0.1}\text{-}[\text{FeTiO}_3]_{0.9}$). (b)–(d) Schematic diagram of the magnetic configuration in the HI-9 system under different external fields. AFM, FM, H , and H_{cr} represent antiferromagnetic, ferromagnetic, external magnetic field, and the critical external magnetic field, respectively.

as the temperature is lower than 30 K [33]. Therefore, the abnormal negative expansions in $\Delta c/c_{300\text{K}}$ are ascribed to the spontaneous magnetostriiction induced by these two types of spontaneous magnetization [44]. As a result, two types of short-range AFM ordering are obtained in HI-9 when the temperature is lower than 30 K. The first is AFM ordering of the Fe^{3+} cations (red) between the neighboring layers, and the second is AFM ordering of the Fe^{2+} cations (orange) between the alternating layers, as shown in the inset of Fig. 2(b).

Figure 2(d) shows the maximum applied magnetic field (H_m) dependence of the hysteresis loop at 5 K, and the inset displays the partially enlarged view. It is observed that the loops are reversibly linear when H_m is lower than 5 kOe, which is consistent with the fact that two types of short-range AFM orderings coexist at 5 K, but the loops begin to show the irreversible hysteresis when H_m is equal to or larger than 5 kOe, which is a typical FM behavior. On the other hand, the rapid linear increase in magnetization from 30 to 40 kOe is also observed, suggesting the existence of AFM ordering. The above results confirm that one type of short-range AFM ordering remains the same, while for the other type of short-range AFM ordering a field-induced dynamic metamagnetic transformation occurs (the critical field is approximately 5 kOe). In principle, the dynamic metamagnetic transformation may occur in the AFM Fe^{3+} sublattice or the AFM Fe^{2+} sublattice, and it

may be the spin-flop transition [45] or the spin-flip transition [46,47]. However, considering that the value of the Néel temperature of $\alpha\text{-Fe}_2\text{O}_3$ (950 K) is much higher than that of isostructural FeTiO_3 (58 K) [33,34], the strength of the AFM ordering of the Fe^{3+} sublattice should be much larger than that of the Fe^{2+} sublattice. Therefore, the dynamic metamagnetic transformation should occur in the AFM Fe^{2+} sublattice. Besides, both magnetization jumps and EB observed in our previous work [31] indicate the existence of the collinear arrangement of magnetic moments, thus the dynamic metamagnetic transformation of the AFM Fe^{2+} sublattice should be the spin-flip transition, as shown in Figs. 1(c) to 1(d). The spin-flip transition of the Fe^{2+} sublattice is crucial for EB because it brings the collinear interface between the Fe^{2+} sublattice and the Fe^{3+} sublattice.

B. Two observed anomalous EB behaviors in HI-9

Figures 3(a)–3(c) show the temperature dependence of H_C , H_E , and the saturation magnetization (M_S) in HI-9, for different values of H_{cool} . It is interesting to observe that both H_C and H_E decrease rapidly with increasing temperature, and they simultaneously reach zero at 30 K. As we know, the other EB systems usually show two other different cases based on the relative anisotropy strength between the pinning and the pinned phases. If the pinning phase has

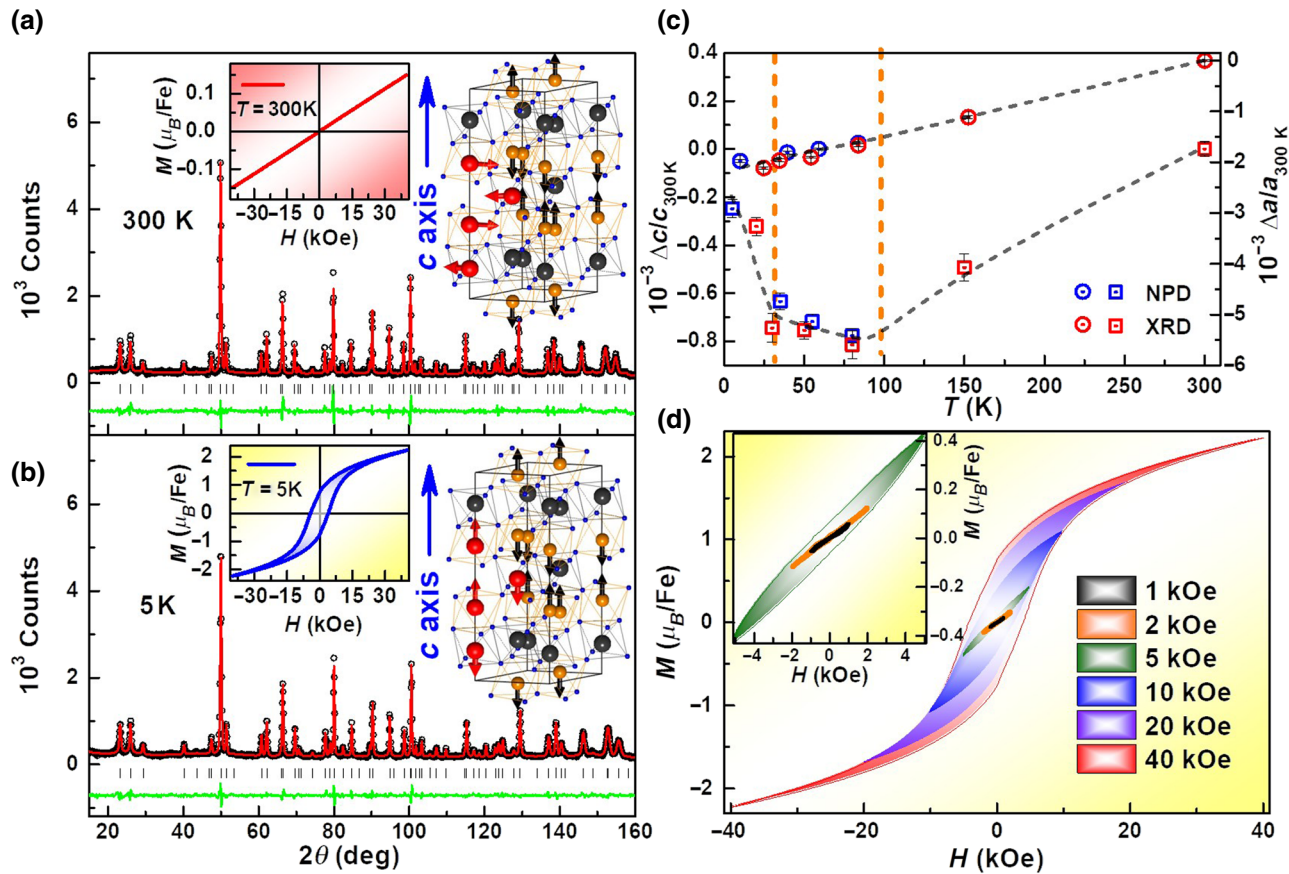


FIG. 2. Three characteristics in HI-9. (a),(b) Neutron powder diffraction patterns of HI-9 at 300 and 5 K. Circles show the experimental intensities (I_{obs}), the red solid line shows the calculated intensities (I_{calc}), the green solid line is the difference between the observed and calculated intensities ($I_{\text{obs}} - I_{\text{calc}}$), and the vertical lines indicate the angular positions of the Bragg reflections. Insets are the magnetic hysteresis loops (left) and the crystal and magnetic structures (right). (c) Temperature dependence of the normalized relative lattice constants ($c - c_{300\text{K}})/c_{300\text{K}} = \Delta c/c_{300\text{K}}$ and $(a - a_{300\text{K}})/a_{300\text{K}} = \Delta a/a_{300\text{K}}$ based on the refinements of the variable-temperature NPD and XRD data, and the dash lines are to guide the eye. (d) Maximum applied magnetic field (H_m) dependence of the magnetic hysteresis loop at 5 K, and H_m is changed from 1 to 40 kOe. Inset displays the partially enlarged view.

a relatively weaker anisotropy, H_C usually reaches its maximum when H_E is reduced to zero, in such a case both the pinning and the pinned phases contribute to H_C . Increasing the temperature [15,48] or decreasing the thickness of the pinning phase [49] is an effective way to reduce the anisotropy of the pinning phase. Whereas if the pinning phase has a relatively stronger anisotropy, there is almost no change in H_C when H_E reduces to zero, in such a case only the pinned phase contributes to H_C [50,51]. Therefore, the correlation between H_C and H_E in HI-9 is completely different from that of the other EB systems, and is regarded as the first anomalous EB behavior of HI-9. In HI-9 the pinned FM Fe^{2+} is not inherent, thus in such a case, it is speculated that only the pinning phase is related to H_C . When the temperature is lower than 30 K, Fe^{3+} transforms from the canted AFM perpendicular to the c axis [see inset of Fig. 2(a)] to the collinear AFM parallel to the c axis [see inset of Fig. 2(b)] [33], i.e., the interface pinning interaction appears. Therefore, both H_C and H_E are completely

originated from the interface pinning interaction, which is completely different from that of the other EB systems. At the same time, it is worth noting that the perpendicular spin coupling between the AFM Fe^{3+} spin and the AFM Fe^{2+} spin cannot generate exchange bias in HI-9. This is different from $\text{Fe}_3\text{O}_4/\text{CoO}$ systems [52–54]. This might due to the absence of the FM Fe^{2+} -spin pinned phase. In addition, it is noticed that both H_C and H_E go to zero at approximately 360 K in the MBE-grown films of $\text{Ni}_{80}\text{Fe}_{20}/\text{FeMn}$ [49]. This behavior is due to the fact that the ordering temperatures of AFM layers and FM layers are approximately 360 K. Obviously, the mechanism in $\text{Ni}_{80}\text{Fe}_{20}/\text{FeMn}$ is different from that in HI-9.

Compared to the case of H_C and H_E , the case of M_S is different. When the temperature is lower than 30 K, M_S is almost unchanged (approximately $2.25 \mu_B/\text{Fe}$); whereas M_S dramatically decreases, when the temperature is higher than 30 K as seen in Fig. 3(c). It is noteworthy that the temperature dependence of M_S is completely different from

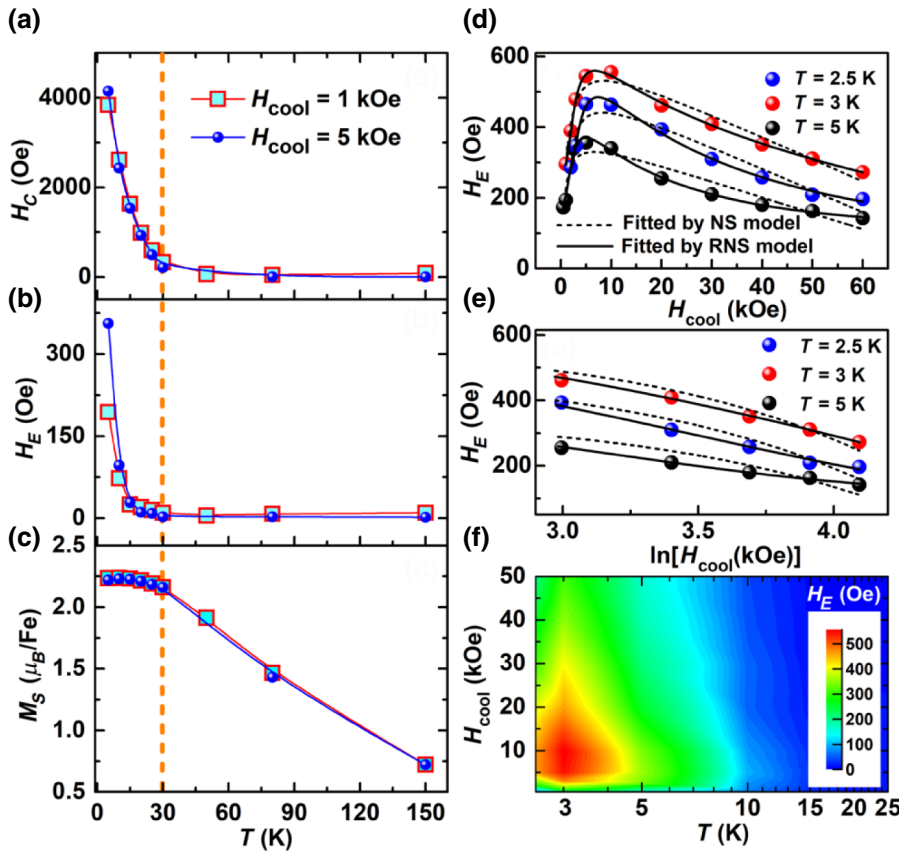


FIG. 3. Two abnormal exchange bias behaviors in HI-9. Temperature dependence of H_C (a), H_E (b), and M_S (c) with different cooling fields ($H_{\text{cool}} = 1$ and 5 kOe). The dotted line shows the position of the $T = 30$ K critical temperature. Cooling field (H_{cool}) (d) and $\ln(H_{\text{cool}})$ (e) dependence of H_E at different temperatures ($T = 2.5, 3$, and 5 K). Dotted lines and solid lines show the fitting results according to the NS model and the RNS model, respectively. (f) Contour map of temperature and cooling field codependence of H_E .

that of H_C and H_E , but the physical mechanism for generating these temperature dependences are the same. They are all due to the disappearance of the collinear AFM-AFM interaction between Fe^{3+} and Fe^{2+} cations and the dynamic magnetic transformation from AFM Fe^{2+} to FM Fe^{2+} . Therefore, it is the collinear AFM-AFM system and the dynamic magnetic transformation that results in the first anomalous EB behavior of HI-9.

Figures 3(d) and 3(e) show the H_{cool} dependence of H_E at different temperatures ($T = 2.5, 3$, and 5 K) in HI-9. With increasing H_{cool} , H_E first increases rapidly when H_{cool} is lower than 10 kOe, then it falls off logarithmically when H_{cool} is higher than 10 kOe as shown in Fig. 3(e) where the horizontal axis is $\ln(H_{\text{cool}})$. The H_{cool} dependence of H_E in HI-9 is also different from that of other EB materials in which H_E either saturates [15] or falls off linearly not logarithmically with further increasing H_{cool} [25,55]. The logarithmic decrease of H_E is thus regarded as the second anomalous EB behavior in HI-9.

For the linear decrease of H_E in other EB materials, Niebieskikwiat and Salamon [56] have put forward a simplified exchange interaction model (referred to below as the NS model) as,

$$-H_E \propto J_i \left[\frac{J_i \mu_0}{(g \mu_B)^2} L \left(\frac{\mu H_{\text{cool}}}{k_B T_f} \right) + H_{\text{cool}} \right], \quad (1)$$

where J_i is the interface exchange constant, g is the Landé factor, μ_B is the Bohr magneton, $L(x)$ is the Langevin function, $\mu = N_v \mu_0$, N_v is the number of FM spins, μ_0 is the vacuum permeability, and k_B is the Boltzmann constant. The dotted lines in Figs. 3(d) and 3(e) show the fitting results according to the NS model. It is seen that there is some deviation between the experimental results and the NS model, maybe due to the field-induced dynamic magnetic transformation in HI-9 as mentioned above. Now the field-induced dynamic magnetic transformation based on the TPPOPP structure is taken into account to modify the NS model. The revised NS model (referred to below as the RNS model) can be expressed as

$$-H_E \propto J_i \left[\frac{J_i \mu_0}{(g \mu_B)^2} L \left(\frac{\mu H_{\text{cool}}}{k_B T_f} \right) + H_{\text{cool}} - \ln(H_{\text{cool}}) \right], \quad (2)$$

where a new term $-J_i \ln(H_{\text{cool}})$ appears compared to the NS model. The detailed derivation of the RNS model is given in part 3 of the Supplemental Material [43]. The solid lines in Figs. 3(d) and 3(e) are the fitting results according to the RNS model. Obviously, the RNS model is in good agreement with the experimental data. It is confirmed that it is the TPPOPP structure and the field-induced dynamic magnetic transformation that leads to the second anomalous EB behavior in HI-9. Figure 3(f) displays the contour

map of temperature and cooling-field codependence of H_E . H_E is extremely sensitive to H_{cool} . H_E will reach its maximum under appropriate temperature and cooling field. This may be correlated to the field-induced dynamic magnetic transformation.

C. Coexistence of first-order magnetic phase transformation and second-order magnetic phase transformation (SOMPT) in HI-9

Both the TPPOPP structure and the two abnormal EB behaviors are correlated to the field-induced dynamic magnetic transformation. Now Arrott plots, in which the initial magnetization data is presented in the form of M^2 versus H/M isotherms, are applied to investigate the field-induced dynamic magnetic transformation in HI-9. If Arrott plots have a negative slope, the transformation is the FOMPT; if Arrott plots show a positive slope, the transformation is the SOMPT [57–59]. Figure 4(a) shows Arrott plots of HI-9 obtained from the initial magnetization curves from 5 to 40 K, which are shown in part 4 of the Supplemental Material [43]. Obviously, except for the 40-K curve, all Arrott plots have both negative and positive slopes, and for each curve, there exists a critical magnetic field (H_{CMF}) represented by the yellow solid circles in Fig. 4(a), at which the slope changes from negative to positive. It is found that for $H < H_{\text{CMF}}$ the slope is negative, i.e., FOMPT occurs; and for $H > H_{\text{CMF}}$ the slope is positive, i.e., SOMPT occurs. FOMPT in the low external field should correspond to the field-induced dynamic magnetic transformation from AFM Fe^{2+} to FM Fe^{2+} [see the left and middle schematic representations in Fig. 4(b)]. Charilaou *et al.* [60] have reported that heat is released during the magnetization jump of Fe^{2+} from AFM to FM. Our result also demonstrates that the transformation of Fe^{2+} in HI-9 is first order. SOMPT in the high external field may correspond to the process of FM Fe^{2+} aligning with the external field direction [see the middle and right schematic representations in Fig. 4(b)]. Therefore, FOMPT and SOMPT coexist in HI-9 when the temperature is lower than 30 K, and only SOMPT exists in HI-9 when the temperature is higher than 30 K.

Figure 4(b) shows the temperature dependence of H_{CMF} . It is seen that H_{CMF} decreases dramatically with increasing temperature and approaches zero at 30 K. This indicates that the external field required to complete FOMPT becomes smaller and smaller, and finally FOMPT disappears for $T > 30$ K. It is noteworthy that with decreasing temperature all anomalies occur at 30 K, including the abnormal negative expansion in the c axis, the Morin transition of Fe^{3+} , exchange bias, coercivity, the constant saturation magnetization, and first-order magnetic transformation. Therefore, all of these are coupled together. The Morin transition of Fe^{3+} leads to the abnormal negative expansion in the c axis, and the emergence of the pinning phase. FOMPT generates FM Fe^{2+} , i.e., the pinned phase.

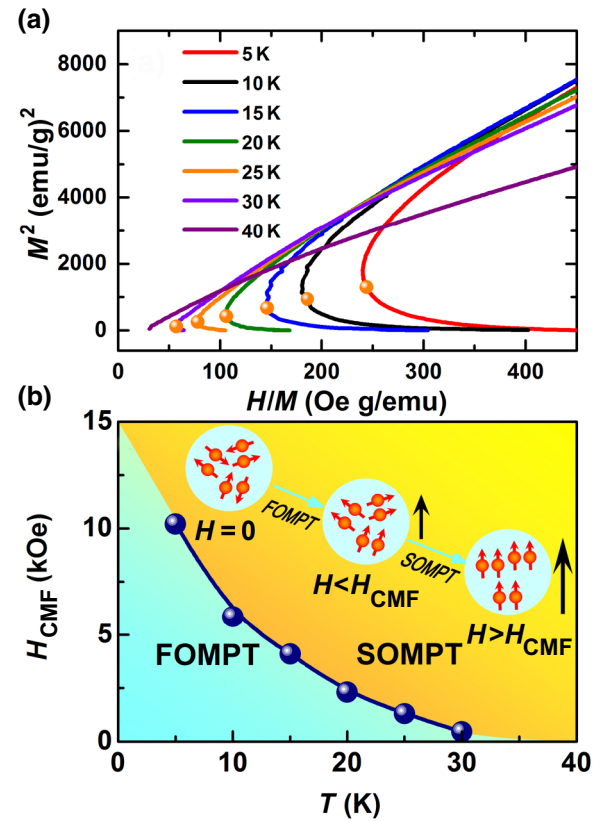


FIG. 4. Field-induced dynamic magnetic transformation in HI-9. (a) Arrott plots from 5 to 40 K. The yellow spheres represent the position of the critical magnetic field (H_{CMF}), where the curve slope changes from negative to positive. (b) Temperature dependence of H_{CMF} . The solid line is to guide the eye. The inset shows the schematic representations of the evolution from the FOMPT to the SOMPT with increasing the external magnetic field. Red and black arrows mark the orientation of the Fe^{2+} moments and the external magnetic field, respectively.

Consequently, the exchange-bias effect (nonzero H_E and H_C) and the constant M_S in HI-9 appear. We conclude, therefore, that it is the Morin transition and FOMPT that cause the anomalous EB behaviors.

IV. CONCLUSION

In summary, $[\alpha\text{-Fe}_2\text{O}_3]_{0.1}[\text{FeTiO}_3]_{0.9}$ (HI-9) can serve as a special platform for investigating exchange-bias effect, due to its three characteristics: (i) an AFM-AFM system, (ii) the “two pinning phases and one pinned phase” structure, and (iii) the field-induced dynamic magnetic transformation between the pinning and pinned phases. These characteristics are supported by the results of the neutron powder diffraction and the magnetic dynamic measurement. Two anomalous EB behaviors are observed in HI-9: (i) both H_C and H_E simultaneously decrease to zero at 30 K due to the collinear AFM-AFM system and the dynamic magnetic transformation, (ii) for a high H_{cool} ,

H_E decreases logarithmically with increasing H_{cool} due to the “two pinning phases and one pinned phase” structure and the field-induced dynamic magnetic transformation, based on which a revised Niebieskikwiat and Salamon model is put forward and it can explain well the logarithmical decrease in H_E . Arrott plots confirm that the FOMPT corresponding to the field-induced dynamic magnetic transformation from AFM Fe²⁺ to FM Fe²⁺ and the SOMPT for the process of FM Fe²⁺ aligning with the external field direction coexist in HI-9. The Morin transition of Fe³⁺ cations and FOMPT cause the anomalous EB behaviors in HI-9. This work may provide fresh ideas for research into the EB effect.

ACKNOWLEDGMENTS

This work is supported by the Hebei Natural Science Foundation (Grants No. A2014205051, No. E2016205268, and No. A2017210070), China Postdoctoral Science Foundation (Grant No. 2016M600192), the Key Project of Natural Science of Hebei Higher Education (Grant No. ZD2017045), and the National Natural Science Foundation of China (Grant No. 11504247). We thank Dr Kewen Shi at Beihang University for help in the refinement of the crystal structure.

- [1] L. W. Martin, Y. H. Chu, Q. Zhan, R. Ramesh, S. J. Han, S. X. Wang, M. Warusawithana, and D. G. Schlom, Room temperature exchange bias and spin valves based on BiFeO₃/SrRuO₃/SrTiO₃/SiBiFeO₃/SrRuO₃/SrTiO₃/Si (001) heterostructures, *Appl. Phys. Lett.* **91**, 172513 (2007).
- [2] P. Borisov, A. Hochstrat, X. Chen, W. Kleemann, and C. Binek, Magnetoelectric Switching of Exchange Bias, *Phys. Rev. Lett.* **94**, 117203 (2005).
- [3] K. Toyoki, Y. Shiratsuchi, A. Kobane, C. Mitsumata, Y. Kotani, T. Nakamura, and R. Nakatani, Magnetoelectric switching of perpendicular exchange bias in Pt/Co/ α -Cr₂O₃/Pt stacked films, *Appl. Phys. Lett.* **106**, 162404 (2015).
- [4] S. S. P. Parkin, K. P. Roche, M. G. Samant, P. M. Rice, R. B. Beyers, R. E. Scheuerlein, E. J. O’Sullivan, S. L. Brown, J. Buccigano, D. W. Abraham, Yu Lu, M. Rooks, P. L. Trouilloud, R. A. Wanner, and W. J. Gallagher, Exchange-biased magnetic tunnel junctions and application to non-volatile magnetic random access memory (invited), *J. Appl. Phys.* **85**, 5828 (1999).
- [5] V. Skumryev, S. Stoyanov, Y. Zhang, G. Hadjipanayis, D. Givord, and J. Nogués, Beating the superparamagnetic limit with exchange bias, *Nature* **423**, 850 (2003).
- [6] D. W. Kavich, J. H. Dickerson, S. V. Mahajan, S. A. Hasan, and J. H. Park, Exchange bias of singly inverted FeO/Fe₃O₄ core-shell nanocrystals, *Phys. Rev. B* **78**, 174414 (2008).
- [7] W. H. Meiklejohn, Exchange anisotropy in the iron-iron oxide system, *J. Appl. Phys.* **29**, 454 (1958).
- [8] V. Papaefthymiou, A. Kostikas, A. Simopoulos, D. Niarchos, S. Gangopadhyay, G. C. Hadjipanayis, C. M. Sorensen, and K. J. Klabunde, Magnetic hysteresis and Mössbauer studies in ultrafine iron particles, *J. Appl. Phys.* **67**, 4487 (1990).
- [9] L. Ma, W. H. Wang, J. B. Lu, J. Q. Li, C. M. Zhen, D. L. Hou, and G. H. Wu, Coexistence of reentrant-spin-glass and ferromagnetic martensitic phases in the Mn₂Ni_{1.6}Sn_{0.4} Heusler alloy, *Appl. Phys. Lett.* **99**, 182507 (2011).
- [10] J. Nogués, T. J. Moran, D. Lederman, I. K. Schuller, and K. V. Rao, Role of interfacial structure on exchange-biased FeF₂-Fe, *Phys. Rev. B* **59**, 6984 (1999).
- [11] Z. J. Guo, J. S. Jiang, J. E. Pearson, S. D. Bader, and J. P. Liu, Exchange-coupled Sm-Co/Nd-Co nanomagnets: Correlation between soft phase anisotropy and exchange field, *Appl. Phys. Lett.* **81**, 2029 (2002).
- [12] M. J. Carey and A. E. Berkowitz, Exchange anisotropy in coupled films of Ni₈₁Fe₁₉ with NiO and Co_xNi_{1-x}O, *Appl. Phys. Lett.* **60**, 3060 (1992).
- [13] B. H. Miller and E. D. Dahlberg, Use of the anisotropic magnetoresistance to measure exchange anisotropy in Co/CoO bilayers, *Appl. Phys. Lett.* **69**, 3932 (1996).
- [14] L. Tang, D. E. Laughlin, and S. Gangopadhyay, Microstructural study of ion-beam deposited giant magnetoresistive spin valves, *J. Appl. Phys.* **81**, 4906 (1997).
- [15] R. D. Hempstead, S. Krongelb, and D. A. Thompson, Unidirectional anisotropy in nickel-iron films by exchange coupling with antiferromagnetic films, *IEEE Trans Magn.* **14**, 521 (1978).
- [16] C. Tsang and Kenneth Lee, Temperature dependence of unidirectional anisotropy effects in the permalloy-FeMn systems, *J. Appl. Phys.* **53**, 2605 (1982).
- [17] J. Nogués and I. K. Schuller, Exchange bias, *J. Magn. Magn. Mater.* **192**, 203 (1999).
- [18] V. Laukhin, V. Skumryev, X. Martí, D. Hrabovsky, F. Sánchez, M. V. García-Cuenca, C. Ferrater, M. Varela, U. Lüders, J. F. Bobo, and J. Fontcuberta, Electric-Field Control of Exchange Bias in Multiferroic Epitaxial Heterostructures, *Phys. Rev. Lett.* **97**, 227201 (2006).
- [19] S. Roy, M. R. Fitzsimmons, S. Park, M. Dorn, O. Petracic, I. V. Roshchin, Z. P. Li, X. Batlle, R. Morales, A. Misra, X. Zhang, K. Chesnel, J. B. Kortright, S. K. Sinha, and I. K. Schuller, Depth Profile of Uncompensated Spins in an Exchange Bias System, *Phys. Rev. Lett.* **95**, 047201 (2005).
- [20] W. H. Meiklejohn, Exchange anisotropy — a review, *J. Appl. Phys.* **33**, 1328 (1962).
- [21] A. E. Berkowitz and K. Takano, Exchange anisotropy — a review, *J. Magn. Magn. Mater.* **200**, 552 (1999).
- [22] A. K. Nayak, M. Nicklas, S. Chadov, C. Shekhar, Y. Skourski, J. Winterlik, and C. Felser, Large Zero-Field Cooled Exchange-Bias in Bulk Mn₂PtGa, *Phys. Rev. Lett.* **110**, 127204 (2013).
- [23] P. J. van der Zaag, R. M. Wolf, A. R. Ball, C. Bordel, L. F. Feiner, and R. Jungblut, A study of the magnitude of exchange biasing in [111] Fe₃O₄/CoO bilayers, *J. Magn. Magn. Mater.* **148**, 346 (1995).
- [24] B. M. Wang, Y. Liu, P. Ren, B. Xia, K. B. Ruan, J. B. Yi, J. Ding, X. G. Li, and L. Wang, Large Exchange Bias After Zero-Field Cooling from an Unmagnetized State, *Phys. Rev. Lett.* **106**, 077203 (2011).

- [25] M. Patra, S. Majumdar, and S. Giri, Grain size effect on the magnetic cluster-glass properties of $\text{La}_{0.88}\text{Sr}_{0.12}\text{CoO}_3$, *J. Phys.: Condens. Matter* **22**, 116001 (2010).
- [26] M. Gruyters, Spin-Glass-Like Behavior in CoO Nanoparticles and the Origin of Exchange Bias in Layered CoO/Ferromagnet Structures, *Phys. Rev. Lett.* **95**, 077204 (2005).
- [27] Z. B. Guo, Y. H. Wu, J. J. Qiu, B. Y. Zong, and G. C. Han, Exchange bias and magnetotransport properties in IrMn/NiFe/FeMn structures, *Phys. Rev. B* **78**, 184413 (2008).
- [28] J. A. De Toro, D. P. Marques, P. Muñiz, V. Skumryev, J. Sort, D. Givord, and J. Nogués, High Temperature Magnetic Stabilization of Cobalt Nanoparticles by an Antiferromagnetic Proximity Effect, *Phys. Rev. Lett.* **115**, 057201 (2015).
- [29] X. Li, K. W. Lin, W. C. Yeh, R. D. Desautels, J. van Lierop, and Philip W. T. Pong, Modulated exchange bias in NiFe/CoO/ α - Fe_2O_3 trilayers and NiFe/CoO bilayers, *Phys. Lett. A* **381**, 524 (2017).
- [30] A. Ponti, A. M. Ferretti, E. Capetti, M. C. Spadaro, G. Bertoni, V. Grillo, P. Luches, S. Valeri, and S. D'Addato, Steering the magnetic properties of Ni/NiO/CoO core-shell nanoparticle films: The role of core-shell interface versus interparticle interactions, *Phys. Rev. Mater.* **1**, 036001 (2017).
- [31] P. Song, G. K. Li, L. Ma, C. M. Zhen, D. L. Hou, W. H. Wang, E. K. Liu, J. L. Chen, and G. H. Wu, Magnetization jumps and exchange bias induced by a partially disordered antiferromagnetic state in $(\text{FeTiO}_3)_{0.9}-(\text{Fe}_2\text{O}_3)_{0.1}$, *J. Appl. Phys.* **115**, 213907 (2014).
- [32] S. A. McEnroe, B. Carter-Stiglitz, R. J. Harrison, P. Robinson, K. Fabian, and C. McCammon, Magnetic exchange bias of more than 1 Tesla in a natural mineral intergrowth, *Nat. Nanotechnol.* **2**, 631 (2007).
- [33] A. H. Morrish, *Canted Antiferromagnetism: Hematite* (World Scientific, Singapore, 1994).
- [34] H. Kato, M. Yamada, H. Yamauchi, H. Hiroyoshi, H. Takei, and H. Watanabe, Metamagnetic phase transitions in FeTiO_3 , *J. Phys. Soc. Jpn.* **51**, 1769 (1982).
- [35] C. Frandsen, B. P. Burton, H. K. Rasmussen, S. A. McEnroe, and S. Mørup, Magnetic clusters in ilmenite-hematite solid solutions, *Phys. Rev. B* **81**, 224423 (2010).
- [36] I. Fita, A. Wisniewski, R. Puzniak, V. Markovich, and G. Gorodetsky, Exchange-bias reversal in magnetically compensated ErFeO_3 single crystal, *Phys. Rev. B* **93**, 184432 (2016).
- [37] I. Fita, A. Wisniewski, R. Puzniak, E. E. Zubov, V. Markovich, and G. Gorodetsky, Common exchange-biased spin switching mechanism in orthoferrites, *Phys. Rev. B* **98**, 094421 (2018).
- [38] A. C. Larson, and R. B. Von Dreele, Los Alamos National Laboratory Report, LAUR 86-748 (2004).
- [39] S. H. Deng, Y. Sun, L. Wang, H. Wu, K. W. Shi, P. W. Hu, Q. Z. Huang, and C. Wang, Near-zero temperature coefficient of resistivity associated with magnetic ordering in antiperovskite $\text{Mn}_{3+x}\text{Ni}_{1-x}\text{N}$, *Appl. Phys. Lett.* **108**, 041908 (2016).
- [40] J. M. De Teresa, C. Ritter, P. A. Algarabel, S. M. Yusuf, J. Blasco, A. Kumar, C. Marquina, and M. R. Ibarra, Detailed neutron study of the crossover from long-range to short-range magnetic ordering in $(\text{Nd}_{1-x}\text{Tb}_x)_{0.55}\text{Sr}_{0.45}\text{MnO}_3$ manganites, *Phys. Rev. B* **74**, 224442 (2006).
- [41] K. W. Shi, Y. Sun, J. Yan, S. H. Deng, L. Wang, H. Wu, P. W. Hu, H. Q. Lu, M. I. Malik, Q. Z. Huang, and C. Wang, Baromagnetic effect in antiperovskite $\text{Mn}_3\text{Ga}_{0.95}\text{N}_{0.94}$ by neutron powder diffraction analysis, *Adv. Mater.* **28**, 3761 (2016).
- [42] B. P. Burton, P. Robinson, S. A. McEnroe, K. Fabian, and T. B. Ballaran, A low-temperature phase diagram for ilmenite-rich compositions in the system $\text{Fe}_2\text{O}_3-\text{FeTiO}_3$, *Am. Mineral.* **93**, 1260 (2008).
- [43] See Supplemental Material at <http://link.aps.org/supplemental/10.1103/PhysRevApplied.11.054018> for the verification of the characteristic temperature, the detailed derivation of the RNS model, and the initial magnetization curves at different temperatures for $[-\text{Fe}_2\text{O}_3]_{0.1}[\text{FeTiO}_3]_{0.9}$.
- [44] S. Chikazumi, *Physics of Ferromagnetism* (Oxford University Press, New York, 1997).
- [45] J. Nogués, L. Morellon, C. Leighton, M. R. Ibarra, and Ivan K. Schuller, Antiferromagnetic spin flop and exchange bias, *Phys. Rev. B* **61**, R6455 (2000).
- [46] Joonghoe Dho, C. W. Leung, Z. H. Barber, and M. G. Blamire, Controlling the exchange interaction using the spin-flip transition of antiferromagnetic spins in $\text{Ni}_{81}\text{Fe}_{19}/\alpha\text{-Fe}_2\text{O}_3$, *J. Appl. Phys.* **97**, 10K101 (2005).
- [47] Joonghoe Dho, C. W. Leung, Z. H. Barber, and M. G. Blamire, Controlling the exchange interaction using the spin-flip transition of antiferromagnetic spins in $\text{Ni}_{81}\text{Fe}_{19}/\alpha\text{-Fe}_2\text{O}_3$, *Phys. Rev. B* **71**, 180402(R) (2005).
- [48] M. Khan, I. Dubenko, S. Stadler, and N. Ali, Exchange bias behavior in Ni-Mn-Sb Heusler alloys, *Appl. Phys. Lett.* **91**, 072510 (2007).
- [49] R. Jungblut, R. Coehoorn, M. T. Johnson, Ch. Sauer, P. J. van der Zaag, A. R. Ball, Th. G. S. M. Rijks, J. aan de Stegge, and A. Reinders, Exchange biasing in MBE-grown $\text{Ni}_{80}\text{Fe}_{20}/\text{Fe}_{50}\text{Mn}_{50}$ bilayers, *J. Magn. Magn. Mater.* **148**, 300 (1995).
- [50] Q. K. Ong, A. Wei, and X. M. Lin, Exchange bias in $\text{Fe}/\text{Fe}_3\text{O}_4$ core-shell magnetic nanoparticles mediated by frozen interfacial spins, *Phys. Rev. B* **80**, 134418 (2009).
- [51] J. H. He, S. L. Yuan, Y. S. Yin, Z. M. Tian, P. Li, Y. Q. Wang, K. L. Liu, and C. H. Wang, Exchange bias and the origin of room-temperature ferromagnetism in Fe-doped NiO bulk samples, *J. Appl. Phys.* **103**, 023906 (2008).
- [52] N. C. Koon, Calculations of Exchange Bias in Thin Films with Ferromagnetic/Antiferromagnetic Interfaces, *Phys. Rev. Lett.* **78**, 4865 (1997).
- [53] Y. Ijiri, J. A. Borchers, R. W. Erwin, and S.-H. Lee, Perpendicular Coupling in Exchange-Biased $\text{Fe}_3\text{O}_4/\text{CoO}$ Superlattices, *Phys. Rev. Lett.* **80**, 608 (1998).
- [54] Y. Ijiri, T. C. Schultheiss, J. A. Borchers, P. J. van der Zaag, and R. W. Erwin, Link Between Perpendicular Coupling and Exchange Biasing in $\text{Fe}_3\text{O}_4/\text{CoO}$ Multilayers, *Phys. Rev. Lett.* **99**, 147201 (2007).
- [55] S. Giri, M. Patra, and S. Majumdar, Exchange bias effect in alloys and compounds, *J. Phys.: Condens. Matter* **23**, 073201 (2011).

- [56] D. Niebieskikwiat and M. B. Salamon, Intrinsic interface exchange coupling of ferromagnetic nanodomains in a charge ordered manganite, *Phys. Rev. B* **72**, 174422 (2005).
- [57] J. Mira, J. Rivas, F. Rivadulla, C. Vázquez-Vázquez, and M. A. López-Quintela, Change from first- to second-order magnetic phase transition in $\text{La}_{2/3}(\text{Ca}, \text{Sr})_{1/3}\text{MnO}_3$ perovskites, *Phys. Rev. B* **60**, 2998 (1999).
- [58] B. S. Wang, C. C. Li, S. Lin, J. C. Lin, L. J. Li, P. Tong, W. J. Lu, X. B. Zhu, Z. R. Yang, W. H. Song, J. M. Dai, and Y. P. Sun, Magnetic properties and room-temperature magnetocaloric effect in the doped antipervoskite compounds $\text{Ga}_{1-x}\text{Al}_x\text{CMn}_3$ ($0 \leq x \leq 0.15$), *J. Magn. Magn. Mater.* **323**, 2017 (2011).
- [59] M. H. Phan, V. Francoa, N. S. Bingham, H. Srikanth, N. H. Hur, and S. C. Yu, Tricritical point and critical exponents of $\text{La}_{0.7}\text{Ca}_{0.3-x}\text{Sr}_x\text{MnO}_3$ ($x = 0, 0.05, 0.1, 0.2, 0.25$) single crystals, *J. Alloys Compd.* **508**, 238 (2010).
- [60] M. Charilaou, K. K. Sahu, S. Zhao, J. F. Löffler, and A. U. Gehring, Interaction-Induced Partitioning and Magnetization Jumps in the Mixed-Spin Oxide $\text{FeTiO}_3-\text{Fe}_2\text{O}_3$, *Phys. Rev. Lett.* **107**, 057202 (2011).